Journal of Glaciology

Article

Cite this article: Ali A, Dunlop P, Coleman S, Kerr D, McNabb RW, Noormets R (2023). Glacier area changes in Novaya Zemlya from 1986–89 to 2019–21 using object-based image analysis in Google Earth Engine. *Journal of Glaciology* **69**(277), 1305–1316. https://doi.org/10.1017/jog.2023.18

Received: 10 October 2022
Revised: 27 January 2023
Accepted: 23 February 2023
First published online: 9 May 2023

Keywords:
Glacier mapping; glacier monitoring; remote sensing

Corresponding author:
Asim Ali; Email: ali-a18@ulster.ac.uk

cambridge.org/jog

Glacier area changes in Novaya Zemlya from 1986–89 to 2019–21 using object-based image analysis in Google Earth Engine

Asim Ali[1], Paul Dunlop[1], Sonya Coleman[2], Dermot Kerr[2], Robert W. McNabb[1] and Riko Noormets[3]

[1]School of Geography and Environmental Sciences, Ulster University, Coleraine, UK; [2]School of Computing, Engineering, and Intelligent Systems, Ulster University, Coleraine, UK and [3]School of Marine, Geology, and Geophysics, University Centre in Svalbard, Longyearbyen, Norway

Abstract

Climate change has had a significant impact on glacier recession, particularly in the Arctic, where glacier meltwater is an important contributor to global sea-level rise. Therefore, it is important to accurately quantify glacier recession within this sensitive region, using multiple observations of glacier extent. In this study, we mapped 480 glaciers in Novaya Zemlya, Russian Arctic, using object-based image analysis applied to multispectral Landsat satellite imagery in Google Earth Engine and quantify the area changes between 1986–89 and 2019–21. The results show that in 1986–89, the total glacierized area was 22 990 ± 301 km^2, in 2000–01 the area was 22 525 ± 308 km^2 and by 2019–21 the glacier area reduced to 21 670 ± 292 km^2, representing a total of 5.8% reduction in glacier area between 1986–89 and 2019–21. Higher glacier area loss was observed on the Barents Sea coast (7.3%) compared to the Kara (4.2%), reflecting previously observed differences in warming trends. The accuracy of the automatically generated outlines of each layer (1986–89, 2000–01 and 2019–21) was evaluated by comparing with manually corrected outlines (reference data) using random sampling, resulting in an overall accuracy estimate of between 96 and 97% compared to the reference data. This automated approach in Google Earth Engine is a promising tool for rapidly mapping glacier change that reduces the amount of time required to generate accurate glacier outlines.

Introduction

Glaciers distinct from the Antarctic and Greenland ice sheets are one of the key elements of the cryosphere and are major freshwater reservoirs (Millan and others, 2022). As a result of climate change, these large freshwater stores are now melting at a fast rate, increasing global sea levels (Zemp and others, 2019; Hugonnet and others, 2021). After thermal expansion, glaciers and ice sheets are the largest contributors to sea-level rise in the 21st century (IPCC, 2021). With millions of people around the world living within a few kilometres of the coast, future sea-level rise has the potential to displace populations across the globe (Kulp and Strauss, 2019).

Over the last few decades the rate of temperature increase in the Arctic has been estimated to be more than twice as high as anywhere else in the world (Schädel and others, 2018; You and others, 2021), with a recent study estimating Artic warming to be as much as four times higher since 1979 (Rantanen and others, 2022). In the Arctic, mountain glaciers, ice caps and the Greenland ice sheet (GrIS) have all retreated over the past 100 years and have started to retreat faster since 2000 (AMAP, 2017). Combined, Arctic glaciers, ice caps and the GrIS contributed ~1.2 mm to sea-level rise each year from 2003 to 2015 (Moon and others, 2019).

Given the importance of glaciers in the Arctic and their potential to impact large parts of the world, it is necessary to develop automated methods that can easily monitor regional glacier changes and provide a clear understanding of the climate change impacts on Arctic glaciers. To monitor changes over such an expansive and largely inaccessible region like the Arctic, satellite remote sensing is an ideal tool as it can be used to map large glacierized areas relatively quickly (e.g. Winsvold and others, 2014).

Several techniques have been used for glacier mapping based on remote-sensing data, such as manual delineation (e.g. Albert, 2002), band ratio (e.g. Bolch and others, 2010), normalized difference snow index (NDSI) (Hall and others, 1995), object-based image analysis (e.g. Robson and others, 2015, 2016) and supervised learning-based classification (e.g. maximum-likelihood, support vector machine and random forest; Nijhawan and others, 2016; Khan and others, 2020; Kumar and others, 2021b). Of these methods, manual delineation is considered to be the most accurate (Albert, 2002; Alifu and others, 2015; Paul, 2017), but this method is both time-consuming and potentially more susceptible to operator bias compared to more automated approaches. Both band ratio and NDSI are well-established, fast and robust methods for mapping debris-free glacier ice over extensive areas (Paul and others, 2015). However, some difficulties are still present in using these index-based methods – for example, mapping glaciers in the presence of lakes, clouds, shadow, seasonal snow and debris cover.

Band ratio with visible and shortwave infrared (SWIR) bands from Landsat imagery (red/SWIR1) is an effective method for mapping shadowed ice, but tends to misclassify lakes (water bodies) as part of the glacier (Kääb and others, 2005; Paul and others, 2007). Band ratio with near infrared (NIR) and SWIR (NIR/SWIR1) have also been used, but using NIR with SWIR is less effective in areas with dark shadows (Burns and Nolin, 2014). NDSI can provide more satisfactory results in the case of shaded ice, but fails to differentiate glacier ice from pro-glacial lakes (Racoviteanu and others, 2008). Supervised learning based classification techniques may have limited applicability over large regions because of the longer processing time (Racoviteanu and others, 2009).

Glacier outlines are an important data source that not only tell us the size of the glacier, but importantly are used for estimating ice volume (Millan and others, 2022) and glacier mass change (Zemp and others, 2019), or predicting sea-level rise (Hock and others, 2019). The Randolph Glacier Inventory (RGI) is a global inventory of glaciers, and it is supplementary to the Global Land Ice Measurements from Space (GLIMS) database (RGI, 2017). GLIMS is an open-access digital database that stores glacier outlines and is a cooperative effort of worldwide institutes (Raup and others, 2007), available at https://www.glims.org/. However, for most glaciers around the world, outlines are only available at a single point in time which limits its use for understanding the long-term impacts of climate change for glaciers in many regions.

In order to map glacier changes over large areas over multiple points in time, multiple satellite images are needed. To do this mapping locally, users must download and store each image, with file sizes ranging from ∼200 MB for complete Landsat 4 and 5 scenes, to ∼1 GB for Sentinel-2 or Landsat 8 and 9 scenes. Processing large images on a desktop or laptop computer can be resource-intensive, which provides an additional cost barrier for large-scale mapping efforts. More recently, cloud-based platforms such as Google Earth Engine (Gorelick and others, 2017) have enabled users to forgo the time and costs of downloading, storing and processing images locally, which has greatly expanded the possibilities for large-scale analysis in a number of fields (e.g. Lea, 2018; Mahdianpari and others, 2020; Zhang and others, 2020).

In this study, a method is developed on the Google Earth Engine cloud-based platform using an object-based image analysis approach to map and generate glacier outlines automatically. We use this method to generate multi-temporal outlines of glaciers on Novaya Zemlya, Russian Arctic. The main goals of this study are: (1) to develop an automated method to map glaciers by leveraging the computational power and extensive data catalogue of Google Earth Engine; (2) to map the glaciers of Novaya Zemlya at multiple points in time; (3) to compare the derived area changes to mass losses (Hugonnet and others, 2021) and (4) to evaluate the accuracy of the method using manually corrected outlines.

Study area

The Russian Arctic consists of three main regions: Franz Josef Land, Severnaya Zemlya and Novaya Zemlya, which lies north of the Russian mainland between the Barents and Kara seas (Grant and others, 2009). According to the RGI version 6.0 (RGI 6.0), the glacier-covered area of Severnaya Zemlya is 16 701 km^2, for Franz Josef Land it is 12 762 km^2 and for Novaya Zemlya it is 22 128 km^2 (RGI, 2017). The most prominent feature of Novaya Zemlya is the large ice cap on the northern island (Severny Island), whereas the southern part of the archipelago (Yuzhny Island) is dominated by small valley and mountain glaciers (Melkonian and others, 2016). The ice cap on the northern side of Novaya Zemlya is ∼400 km long and has a maximum elevation of 1600 m above sea level (a.s.l.), with the southern part of Novaya Zemlya reaching 1340 m a.s.l. (Rastner and others, 2017).

Novaya Zemlya (Fig. 1) has three different types of glaciers: the main ice cap's large outlet glaciers are mostly marine-terminating, while most of the glaciers that are separated from the main ice cap are land-terminating, with a small number of lake-terminating glaciers (Rastner and others, 2017). According to the RGI 6.0, Novaya Zemlya has a total of 480 glaciers: 38 marine-terminating glaciers, 424 land-terminating glaciers and 18 lake-terminating glaciers.

Data and methods

Data

Landsat images have proven to be an effective asset for glacier mapping, and for creating multi-temporal outlines of glaciers due to its large swath width, its multispectral capabilities and its long temporal record of capturing images for over five decades (e.g. Nuth and others, 2013). A total of 16 images from Landsat 5 Thematic Mapper (TM), Landsat 7 Enhanced Thematic Mapper Plus (ETM+) and Landsat 8 Operational Land Imager (OLI) are used in this study (Table 1), divided into three time periods: 1986–89, 2000–01 and 2019–21. The images used were carefully selected with minimal cloud cover.

Landsat is a collaborative effort of the USGS and NASA and has been continuously observing the Earth from 1972 until the present day (Wulder and others, 2022). The USGS provides Landsat products in three categories: real-time (RT), tier 1 and tier 2 which are stored in Collection 1 or 2. Tier 1 images have the best quality, and are considered suitable for time-series analysis (Masek and others, 2020), while tier 2 images have issues with geometric correction but are still usable. In this study, we use orthorectified level-2 (surface reflectance) images (tier 1) from Collection 1 for mapping glaciers in Novaya Zemlya. Some studies have used raw radiance or digital number (DN) values for glacier mapping with no atmospheric or topographic correction (Paul and others, 2002; Alifu and others, 2015). However, surface reflectance data are essential for systematic analysis, particularly in highly automated approaches (Hemati and others, 2021).

Method

Google Earth Engine is a cloud-based remote-sensing platform with planetary-scale analysis capabilities that contains a multi-petabyte catalogue of satellite imagery and geospatial datasets, making Google Earth Engine one of the most powerful remote-sensing analysis tools available for analysing change datasets (Gorelick and others, 2017). Using Google Earth Engine, we developed an object-based image analysis approach for classifying imagery, instead of a simpler pixel-based approach. Pixel-based classification focuses on individual pixels and neglects additional contextual information contained in surrounding pixels that could be used to increase the accuracy such as the spatial relationship with surrounding pixels, size of objects, texture and shape that object-based image analysis incorporates (Blaschke, 2010).

The method was initially developed using a single Landsat 8 OLI/TIRS image before being applied to the other image sets for the whole of Novaya Zemlya to map glacier changes. This study utilizes six bands from visible to SWIR (OLI bands 2–7), and one thermal infrared band (TIR; TIRS band 10) as input layers for image segmentation (Fig. 2). The visible to SWIR

https://doi.org/10.1017/jog.2023.18 Published online by Cambridge University Press

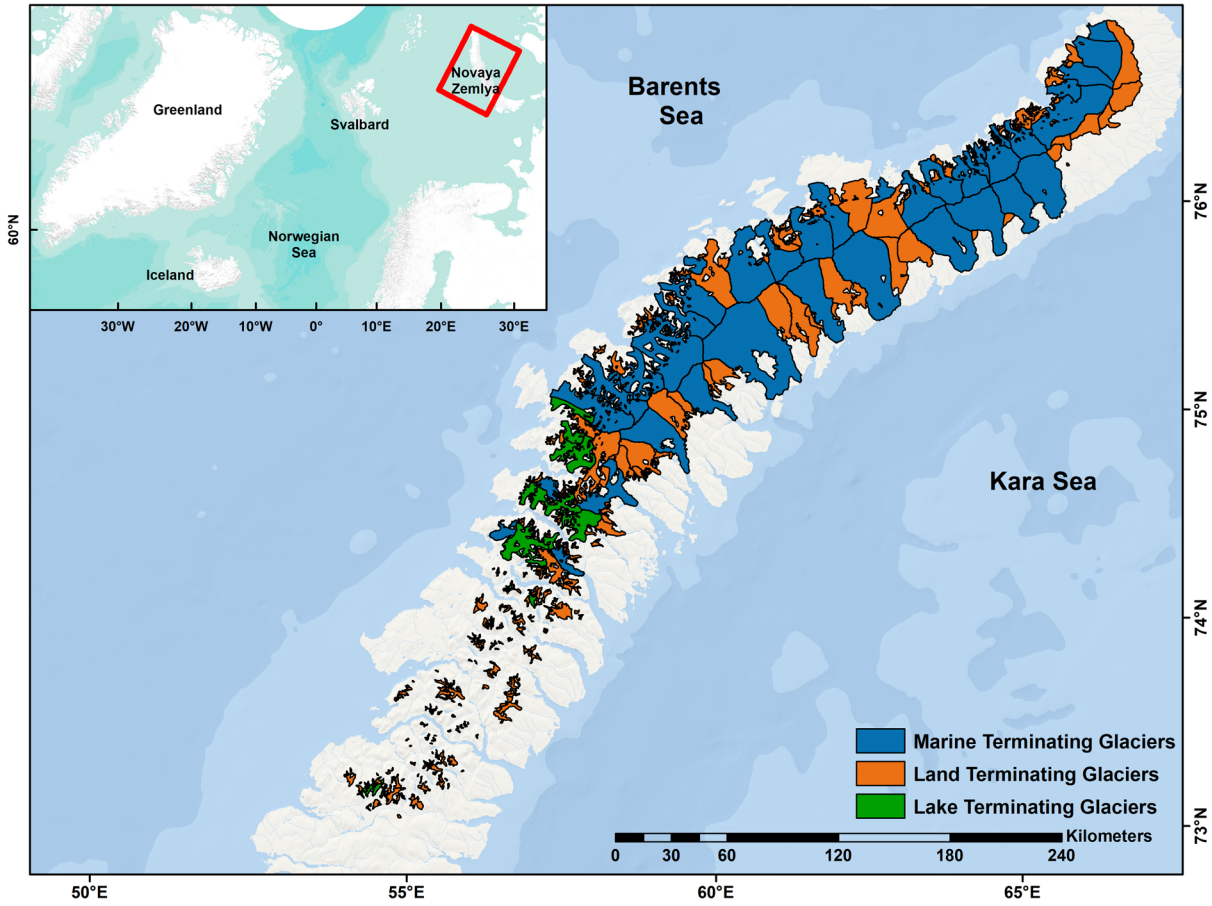

Figure 1. Study area of Novaya Zemlya, with RGI 6.0 glacier outlines shown. The ESRI World Ocean and World Terrain basemaps are used in the background.

Table 1. Details of the Landsat images that are used in this study

Sl. No.	Satellite	Date (DD/MM/YYYY)	WRS-2 path/row	Google Earth Engine image IDs
01	Landsat 5	26/07/1986	174/6	LANDSAT/LT05/C01/T1_SR/LT05_174006_19860726
02	Landsat 5	03/08/1987	177/6	LANDSAT/LT05/C01/T1_SR/LT05_177006_19870803
03	Landsat 5	06/08/1989	179/6	LANDSAT/LT05/C01/T1_SR/LT05_179006_19890806
04	Landsat 5	06/08/1989	179/7	LANDSAT/LT05/C01/T1_SR/LT05_179007_19890806
05	Landsat 5	06/08/1989	179/8	LANDSAT/LT05/C01/T1_SR/LT05_179008_19890806
06	Landsat 7	25/08/2000	174/6	LANDSAT/LE07/C01/T1_SR/LE07_174006_20000825
07	Landsat 7	31/07/2000	175/6	LANDSAT/LE07/C01/T1_SR/LE07_175006_20000731
08	Landsat 7	12/08/2000	179/6	LANDSAT/LE07/C01/T1_SR/LE07_179006_20000812
09	Landsat 7	12/08/2000	179/7	LANDSAT/LE07/C01/T1_SR/LE07_179007_20000812
10	Landsat 7	08/08/2001	178/8	LANDSAT/LE07/C01/T1_SR/LE07_178008_20010808
11	Landsat 8	20/08/2019	176/5	LANDSAT/LC08/C01/T1_SR/LC08_176005_20190820
12	Landsat 8	20/08/2019	176/6	LANDSAT/LC08/C01/T1_SR/LC08_176006_20190820
13	Landsat 8	23/08/2021	178/7	LANDSAT/LC08/C01/T1_SR/LC08_178007_20210823
14	Landsat 8	18/08/2020	180/6	LANDSAT/LC08/C01/T1_SR/LC08_180006_20200818
15	Landsat 8	19/09/2020	180/7	LANDSAT/LC08/C01/T1_SR/LC08_180007_20200919
16	Landsat 8	19/09/2020	180/8	LANDSAT/LC08/C01/T1_SR/LC08_180008_20200919

bands have 30 m resolution. The TIR band was originally collected with 100 m resolution, but Google Earth Engine automatically resampled this using a cubic convolution method to 30 m.

In the object-based image analysis approach, segmentation is an important step that groups similar pixels into a cluster or image objects (Ren and Malik, 2003). Pixel-based classification can result in so-called 'salt and pepper' noise, and segmentation helps to reduce this effect in the final classification (Ma and others, 2019). To reduce noise in the images, a one-sigma Gaussian filter of radius 2 was applied before segmentation (Xue and others, 2018).

Google Earth Engine mainly supports three image segmentation techniques for remote sensing: simple non-iterative clustering, *k*-means and *G*-means (Liu and others, 2018). We use simple non-iterative clustering (Achanta and Süsstrunk, 2017), which is an improved version of simple linear clustering, to segment the Landsat image (Fig. 3b). The important parameters of simple non-iterative clustering are compactness, connectivity, seeds or grid size and neighbourhood size. The compactness parameter defines the smoothness of the clusters, which affects cluster shape (Shafizadeh-Moghadam and others, 2021). A compactness value of zero removes spatial distance weighting, meaning that clusters are created based only on spectral characteristics. The connectivity parameter deals with adjacent objects, with a connectivity of four corresponding to only orthogonal neighbours, and a connectivity of eight corresponding

https://doi.org/10.1017/jog.2023.18 Published online by Cambridge University Press

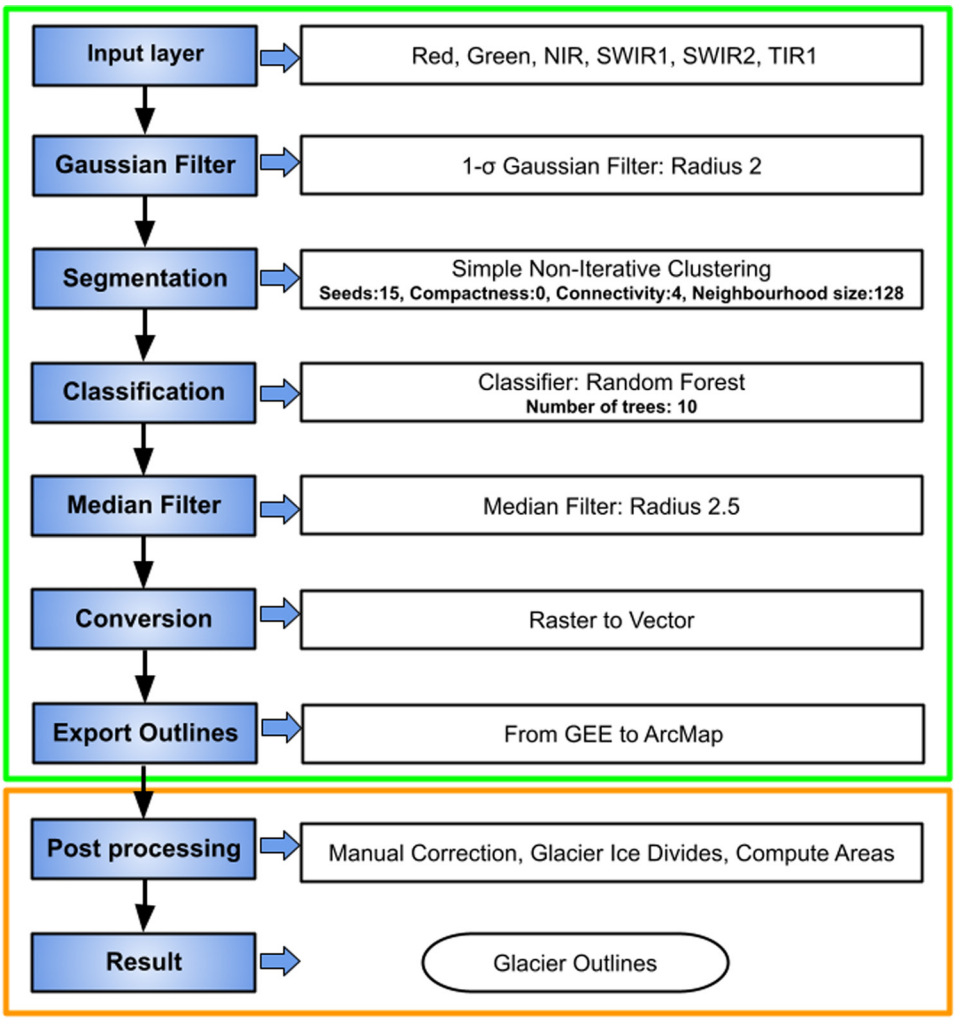

Figure 2. Workflow of the method for creating glacier outlines in Google Earth Engine. The green box shows the automated steps in Google Earth Engine, while the orange box shows the post-processing steps in ArcMap 10.5.1.

to orthogonal and diagonal neighbours. The seed/size parameter determines the initial location or spacing of the cluster centres, and neighbourhood size is used to avoid boundary artefacts between tiles (Tassi and Vizzari, 2020). In this study, the parameters compactness = 0, connectivity = 4, seed grid spacing of 15 pixels and neighbourhood size = 128 pixels were selected by repeated iteration and visual evaluation.

The random forest classifier was implemented in Google Earth Engine for the classification of the segmented image. The random forest algorithm is a supervised machine learning algorithm that combines the output of multiple decision trees to produce a single result (Kulkarni and Lowe, 2016). For image classification, random forest is the most widely used machine learning algorithm in Google Earth Engine (Amani and others, 2020). Random forest

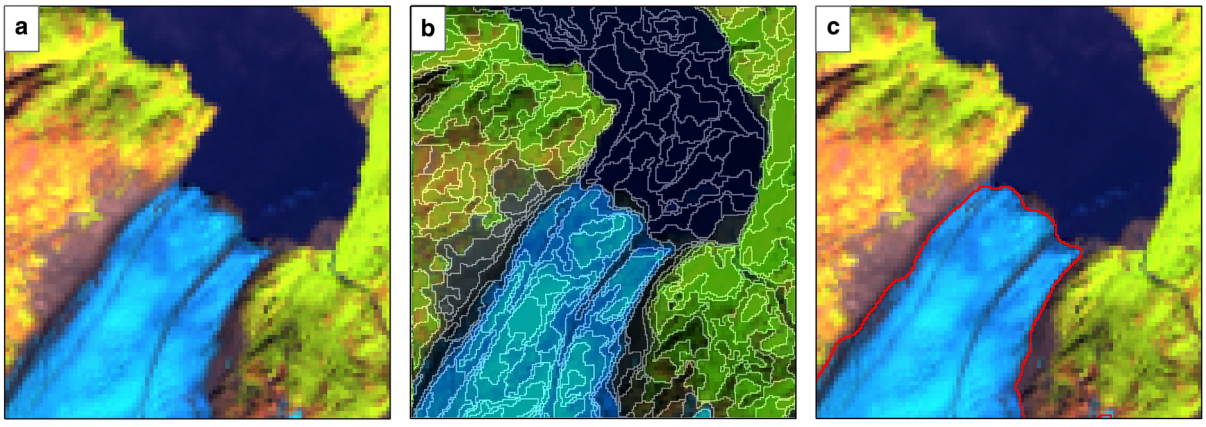

Figure 3. Process of generating outlines using an object-based image analysis approach in Google Earth Engine: (a) a false colour composite of a Landsat 8 image (OLI bands SWIR1, NIR and red); (b) the result of simple non-iterative clustering segmentation and (c) the final glacier outline, overlain on the original image.

https://doi.org/10.1017/jog.2023.18 Published online by Cambridge University Press

is robust, easier to implement, capable of dealing with high dimensionality and can reduce the risk of overfitting (Nery and others, 2016; Praticó and others, 2021).

In this study, the random forest algorithm using ten trees was trained on manually selected samples of 'glacier' and 'non-glacier' throughout the scene, and the segments were classified into two main classes: 'glacier' and 'non-glacier'. The 'glacier' class includes ice, debris-covered ice and moraines, while the non-glacier class includes water, vegetation, sea-ice, bare land and seasonal snow patches. To train the classifier, we used a total of 728 samples for the 1986–89 images, including 365 glacier samples and 363 non-glacier samples. For the 2000–01 images, we used 317 glacier and 303 non-glacier samples and for the 2019–21 images we used 339 glacier and 367 non-glacier samples.

Finally, a median filter with radius 2.5 was applied to reduce noise in the classified image, and the classified image was converted from raster to vector to create glacier outlines (Fig. 3c). The automated glacier outlines were exported from Google Earth Engine to ArcMap 10.5.1 for post processing. As a final step, each glacier was visually examined to see if manual correction was required, and manual corrections were made where necessary. Finally, the linked glacier outlines were separated using the internal boundaries of the RGI 6.0, to enable examination of the changes in each glacier.

Accuracy and uncertainty

The temporal nature by which satellite images are captured invariably means that images of the same area are captured during different conditions, and there can be seasonal variations that can impact image quality. These variations can be illumination differences, cloud cover or shadows cast over the target feature; for glacier mapping, seasonal snow patches can remain on the ground which are spectrally similar to snow-covered glaciers. Because of this, it is important to understand the capabilities of the method when utilizing images from different times and to assess how accurate the glacier areas are computed using this automated methodology without manual corrections. Therefore, to determine the uncertainty in the glacier area, two approaches were used: random sampling and buffer analysis.

Uncertainty by random sampling

To assess the accuracy of the automated outlines from each period, random samples were generated for each class in ArcMap 10.5.1, using the manually corrected outlines as reference data. The random samples were separated into two classes: 'glacier' and 'non-glacier', with an equal number of samples for each class. In total, 1998 samples for each class were taken for the 1986–89 outlines; 1971 samples from each class for the 2000–01 outlines and 1937 samples from each class for the 2019–21 outlines. These points were intersected with the automatically generated outlines and the reference data, and confusion matrices were created (Table 2).

Uncertainty using buffer analysis

To assess the area uncertainty of the manually corrected outlines, a buffer of ±30 m was applied to each manually corrected layer. In the absence of suitable reference data, the buffer approach is typically employed to determine accuracy using a literature-derived uncertainty value (±0.5 or 1 pixel; Granshaw and Fountain, 2006; Paul and others, 2017). The uncertainty in the glacier area was determined by calculating the buffered area of each layer. The high, low and area ± uncertainty values for each period are shown in Table 3.

Table 2. Confusion matrices of each layer generated based on random sampling

	Reference data				
	Glacier	Non-glacier	Total	User's accuracy	Kappa
1986–89					
Classified					
Glacier	1973	100	2073	95.1%	0.93
Non-glacier	25	1898	1923	98.7%	
Total	1998	1998	3996		
Producer's accuracy	98.7%	94.9%			
2000–01					
Classified					
Glacier	1954	140	2094	93.3%	0.92
Non-glacier	17	1831	1848	99.0%	
Total	1971	1971	3942		
Producer's accuracy	99.1%	92.8%			
2019–21					
Classified					
Glacier	1917	115	2032	94.3%	0.93
Non-glacier	20	1822	1842	98.9%	
Total	1937	1937	3874		
Producer's accuracy	98.9%	94.0%			

Results

In 1986–89, the total glacierized region of Novaya Zemlya was 22 990 ± 301 km^2, in 2000–01 the area was 22 525 ± 308 km^2 and by 2019–21 the glacier area was reduced to 21 670 ± 292 km^2. Of the 480 glaciers mapped, 142 are >10 km^2, 262 glaciers are between 1 and 10 km^2 and 76 glaciers are <1 km^2. This glacier inventory includes three terminus types: 38 marine-terminating, 424 land-terminating and 18 lake-terminating glaciers. The marine-terminating glaciers cover the most glacier area (14 448 ± 137 km^2), followed by the land-terminating glaciers covering 7299 ± 94 km^2 and the lake-terminating glaciers that cover 1241 ± 16 km^2.

The overall accuracy for each layer was calculated using the confusion matrices (Table 2). The 1986–89 layer showed 96.8% overall accuracy, the 2000–01 layer had 96.0% accuracy and the 2019–21 layer had 96.5% accuracy. The details of producer's and user's accuracy are mentioned in Table 2. The producer's accuracy varies between 92.8 and 98.9%, the user's accuracy ranges between 93.3 and 99.0% and the kappa coefficient is ⩾0.92 for all three layers.

It is also important to assess how accurate the automatically generated glacier areas are, using the information displayed in Table 2. Table 4 compares the manually estimated glacier areas with the unbiased estimates of glacier area for each time period, calculated following the methods described by Olofsson and others (2013). The comparison of manual and automated area estimates shows that besides 2000–01, the manual and automated area estimates overlap within the uncertainty bands. When compared to 1986–89 and 2000–01, the manual area estimate shows that the area loss nearly doubled between 2000–01 and 2019–21, whereas the automatic estimate shows the opposite. Additionally, the automated estimate of the area change between 2000–01 and 2019–21 has a larger uncertainty (±624 km^2) than the estimated change (−441 km^2).

Table 3. Computed areas (in km^2) of each layer based on the ±30 m buffer

Time period	High	Low	Area
1986–89	23 291	22 689	22 990 ± 301
2000–01	22 833	22 217	22 525 ± 308
2019–21	21 962	21 378	21 670 ± 292

https://doi.org/10.1017/jog.2023.18 Published online by Cambridge University Press

Table 4. Total area (in km^2) of glaciers computed from manually corrected outlines (±1 pixel buffer), both including and excluding glaciers that surged, and the automatically generated outlines (±95% confidence interval)

	Manual		Change (from previous)			
	All	Non-surge	All	Non-surge	Automated	Change (from previous)
1986–89	22 990 ± 301	22 049 ± 301			22 930 ± 470	
2000–01	22 525 ± 308	21 578 ± 308	−465 ± 430	−470 ± 430	21 762 ± 435	−1168 ± 640
2019–21	21 670 ± 292	20 756 ± 292	−855 ± 424	−821 ± 424	21 321 ± 448	−441 ± 624

Glacier area changes

To calculate area changes, we use the manually corrected glacier outlines. Between 1986–89 and 2019–21, glaciers in Novaya Zemlya showed a 5.8% reduction in total area. Glacier retreat rates increased by 1.7% from 2000–01 to 2019–21 (−3.8%), compared to from 1986–89 to 2000–01 (−2.1%). These changes in glacier area were not constant across glacier terminus type (land-, lake- and marine-terminating). From 1986–89 to 2019–21, land-terminating glaciers lost 580 ± 130 km^2 (7.9%), lake-terminating glaciers lost 106 ± 21 km^2 (9.9%), and marine-terminating glaciers lost 605 ± 263 km^2 (4.4%) of glacierized area (Fig. 4).

Figure 5a depicts the area lost for each glacier from 1986–89 to 2000–01 and Figure 5b shows the loss of each glacier from 2000–01 to 2019–21, while Figures 5c,d show the area loss of each glacier as a percentage. Only 41 glaciers larger than 200 km^2 are responsible for nearly half (49.5%) of the area loss in the region, and 272 glaciers are responsible for 84% of the total glacier area loss. Because of the larger area of these glaciers, however, the total percentage loss for these 272 glaciers is <25%.

Figure 6 shows the per cent area change vs glacier area based on terminus type. Figure 6b depicts 38 marine-terminating glaciers that cover the majority of the glacierized region (14 448 ± 137 km^2) in Novaya Zemlya, Figure 6a shows 18 lake-terminating glaciers which cover 1241 ± 16 km^2, while Figure 6c shows 424 land-terminating glaciers covering 7299 ± 94 km^2. In between 1986–89 and 2019–21, three land-terminating glaciers have completely disappeared, and 18 glaciers retreated more than 60%, while a further 57 glaciers retreated between 40 and 60%.

Discussion

Glacier retreat

As reported elsewhere (e.g. Sharp and others, 2014; Kochtitzky and Copland, 2022), it is clear that glaciers are retreating across the Arctic. This study shows that all glaciers in Novaya Zemlya have retreated at various rates from 0.3 to 100%, with a few examples of surging glaciers captured in the analysis (Figs 5a, c). Although the area loss of glaciers differed by each glacier type in Novaya Zemlya. Carr and others (2017) found that the retreat rate of marine-terminating glaciers is higher than that of land-terminating glaciers, which is corroborated by our results (Fig. 4). However, land-terminating glaciers did not experience the same increase in retreat rate as lake- and marine-terminating glaciers in 2000–01 to 2019–21. The retreat rate of land-terminating glaciers increased by 1.4% between 2000–01 and 2019–21 relative to that between 1986–89 and 2000–01, whereas the retreat rates of lake- and marine-terminating glaciers increased by 2.8 and 1.7%, respectively.

Like the rest of the Arctic, Novaya Zemlya is warming faster than the rest of the world, with both surface air and sea surface temperatures increasing rapidly over both the Barents and Kara Sea coasts (e.g. Kohnemann and others, 2017; Isaksen and others, 2022). In particular, Isaksen and others (2022) found that 2 m surface air temperature warming was higher on the Barents Sea side of Novaya Zemlya (1.5–2.0°C decade^{-1} between 1981–2020) compared to the Kara Sea side (1.0–1.5°C decade^{-1}). These changes are driven in part by a decrease in sea ice concentration (SIC) in the region (Yamagami and others, 2022), with the drop in SIC over the Barents Sea nearly twice as high compared to the Kara Sea (Kumar and others, 2021a). Consistent with these studies, our observations show that glaciers terminating on the Barents Sea coast of Novaya Zemlya retreated faster than glaciers terminating on the Kara Sea coast (Fig. 7), a pattern that remains consistent across glacier terminus type (Fig. 8). Barents Sea glaciers lost a total area of 843.4 km^2 (−7.3%) between 1986–89 and 2019–21, while glaciers on the Kara Sea lost 448.9 km^2 (−4.2%).

Examination based on terminus type shows that all three types of glaciers are retreating more on the Barents Sea side than those terminating on Kara Sea side (Fig. 8). Carr and others (2014) observed a similar pattern of higher retreat on the Barents Sea coast than the Kara Sea between 1992 and 2010. Marine- and lake-terminating glaciers are retreating faster on both sides, in both time periods of the study, although land-terminating glacier retreat is slowing down at the Barents Sea in 2000–01 to 2019–21 compared to 1986–89 and 2000–01.

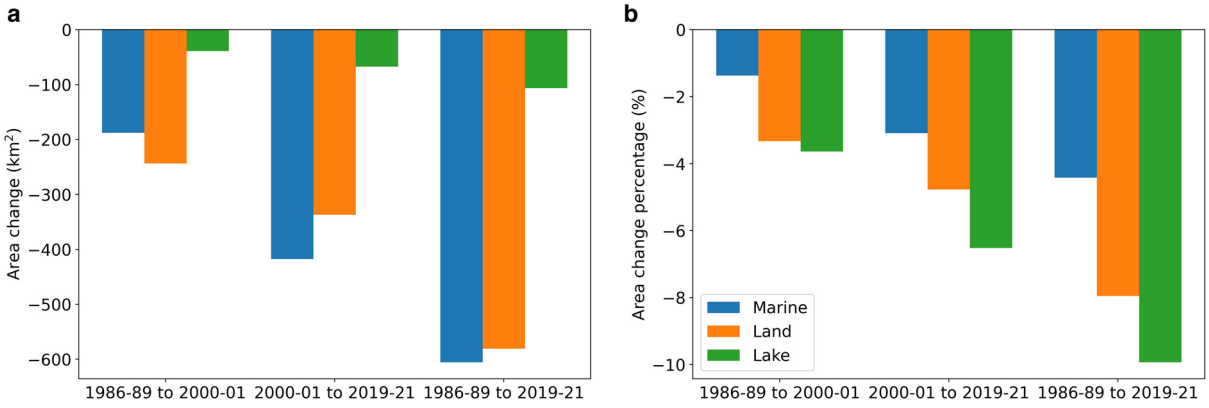

Figure 4. Total area change for lake, marine and land-terminating glaciers in both km^2 (a) and per cent area (b).

https://doi.org/10.1017/jog.2023.18 Published online by Cambridge University Press

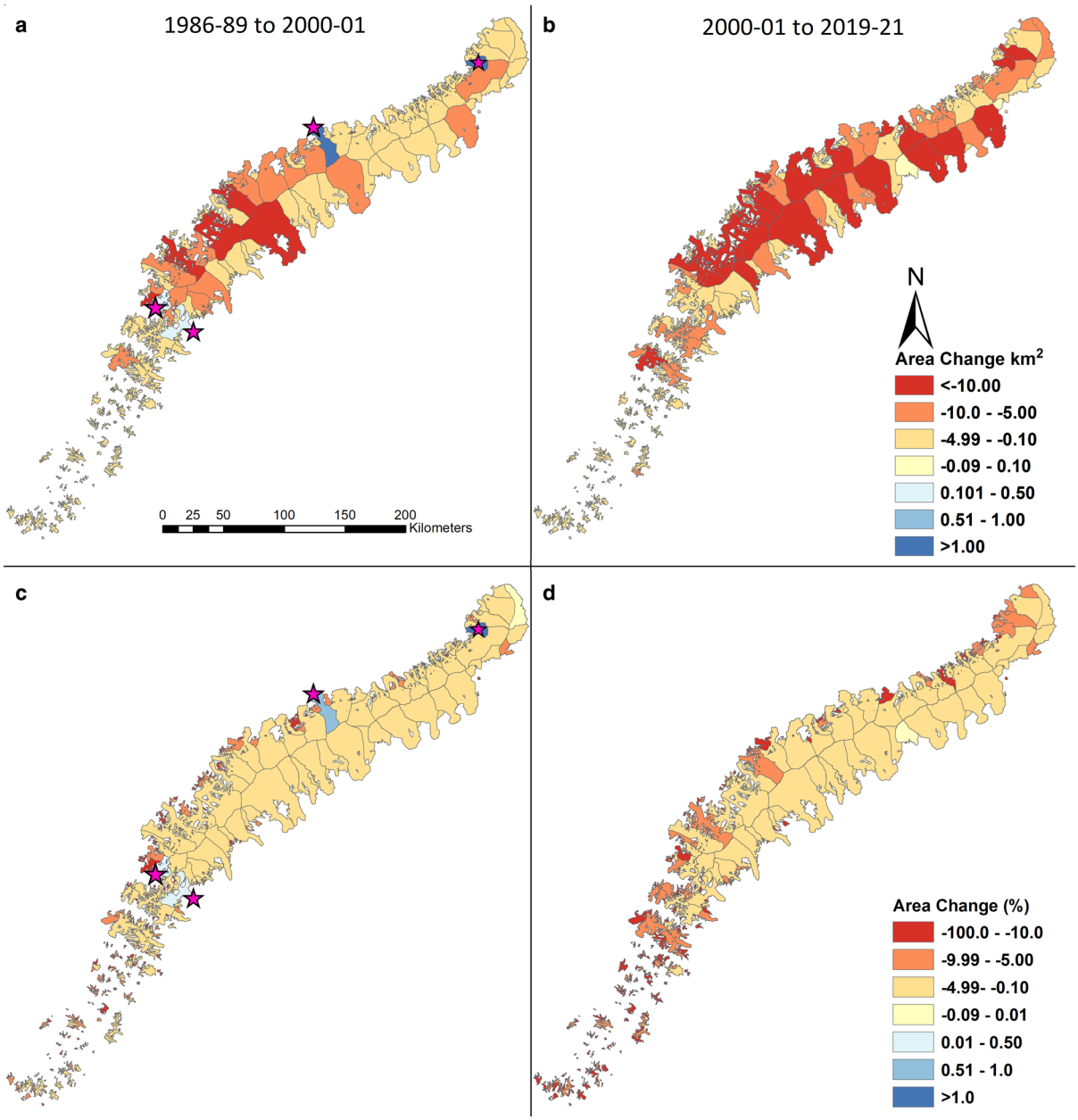

Figure 5. Area changes of Novaya Zemlya glaciers: (a) from 1986–89 to 2000–01 and (b) 2000–01 to 2019–21 in km^2, and (c) from 1986–89 to 2000–01 and (d) 2000–01 to 2019–21 as a per cent. Stars in (a) and (c) show glaciers that surged during the 1986–89 and 2000–01 period.

All three types of glaciers: lake-, marine-, and land-terminating have lost more glacier area from 2000–01 to 2019–21 than 1986–89 to 2000–01; although, during the period 1986–89 to 2000–01, three marine-terminating glaciers and one lake-terminating glacier surged. Two of the same glaciers were identified by Carr and others (2017), and one was identified by Grant and others (2009). This study identified one additional glacier surge (Pavlov Glacier, RGI 6.0 ID: RGI60-09.00070) that increased the area of the glacier by 3.2 km^2, and showed terminus advance by up to 1.3 km by 2000–01 compared to 1986–89 (Fig. 9). No glacier surges were observed in the land-terminating glaciers. During 1986–89 to 2000–01, all four surged glaciers increased in area by 0.6% (+5.8 km^2), however during the second time period (2000–01 to 2019–21), the same glaciers retreated and showed a strongly negative change in area of −3.4% (−32.6 km^2), with a net area loss between 1986–89 and 2019–21 for each glacier. These four glacier were excluded from the area change analysis.

Comparison of glacier area loss with mass-balance loss

Comparing glacier area changes with geodetic mass balances obtained from Hugonnet and others (2021) for the period 2000–20 shows that marine-terminating glaciers lost both area (3.1%) as well as mass (−0.25 m a^{-1}) and lake-terminating glaciers lost a total of 6.5% area while also showing greater mass loss (−0.42 m a^{-1}) compared to land- and marine-terminating glaciers (Fig. 10). However, land-terminating glaciers show a slightly different pattern than lake- and marine-terminating glaciers (Fig. 10), with land-terminating glaciers losing a substantial amount of area (4.7%) with less substantial mass loss (−0.18 m a^{-1}).

Figure 11 depicts a comparison of each glacier area loss with its mass loss. The results indicate that lake-terminating glaciers lost more area than land and marine-terminating glaciers (Fig. 10), with a more negative mass balance (Fig. 11). Ciracì and others (2018) found that marine-terminating glaciers are losing mass faster than glaciers terminating on land. Almost the same trend can

https://doi.org/10.1017/jog.2023.18 Published online by Cambridge University Press

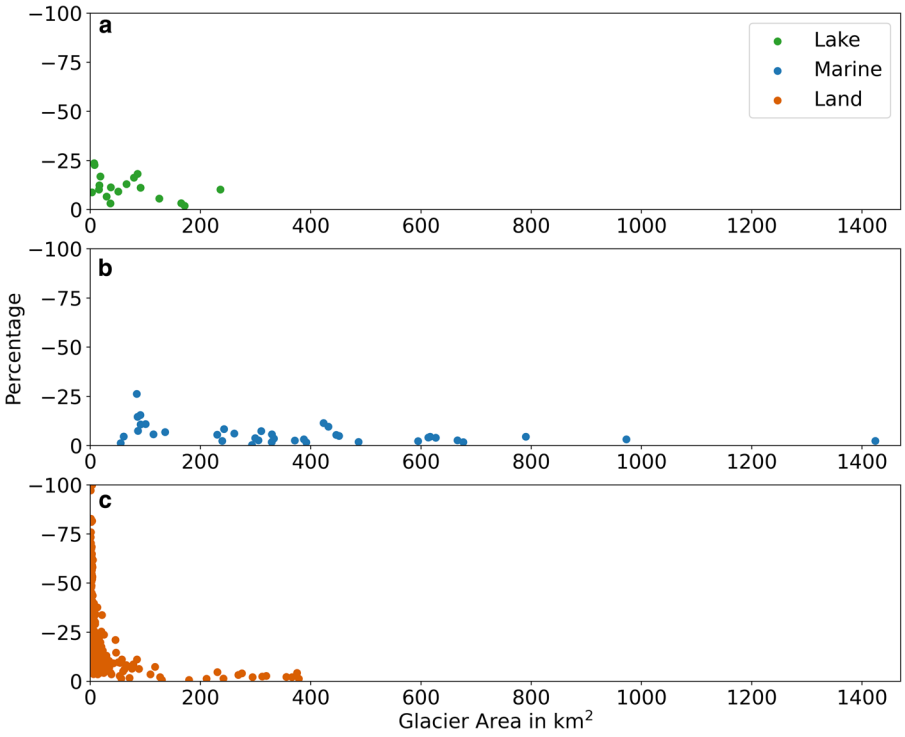

Figure 6. Per cent area change vs glacier area for each glacier from 1986–89 to 2019–21, for (a) lake-terminating, (b) marine-terminating and (c) land-terminating glaciers.

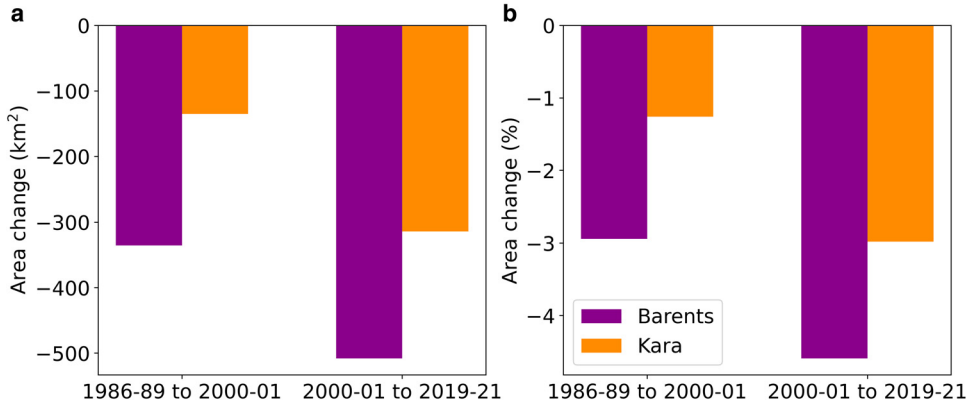

Figure 7. Area change for glaciers on the Barents Sea vs Kara Sea (a) in km^2 and (b) as a percentage.

be seen in marine-terminating glaciers, with a more negative area-averaged mass balance for marine-terminating glaciers compared to land-terminating glaciers (Fig. 11), because marine- and lake-terminating glaciers lose mass via frontal ablation and land-terminating glaciers do not. Land-terminating glaciers showed the least mass loss compared to marine- and lake-terminating glaciers, as seen in the total mass loss of land-terminating glaciers (Fig. 10). In terms of relative area change, however, land-terminating glaciers showed a stronger decrease in area compared to marine-terminating glaciers.

Methodology framework in Google Earth Engine

Rastner and others (2013) compared object-based image analysis with pixel-based classification using the red/SWIR band ratio technique, demonstrating that object-based image analysis performed better than pixel-based classification and reduced the time needed for manual corrections, despite the longer processing time required.

The 16 level-2 products used in this study total 9.10 GB as distributed by USGS Earth Explorer. Downloading the files via the USGS Bulk Download Web Application took ~15 min, even on a fast internet connection. In comparison, running the script to generate outlines for a single image on Google Earth Engine and exporting the outlines took ~1 min.

In addition to the time saved by forgoing downloading and processing the images locally, the object-based image analysis method implemented on Google Earth Engine reduced the amount of manual correction needed when compared to the red/SWIR1 band ratio method. Figure 12 compares the object-based image analysis output to the manually corrected outlines, as well as the output of the red/SWIR1 band ratio using a threshold of 2.0, following Rastner and others (2017). Both outputs clearly require manual correction, with large areas of seasonal snow captured by both methods in the area shown in Figure 12a, but the band ratio output captures a large area of seasonal and perennial snow patches (Fig. 12b) that is not captured by the object-based image analysis output. In addition, both methods have misclassified areas of thin cloud cover, shown in the middle of Figure 12b, as well as areas with larger medial moraines.

In this study, the Google Earth Engine object-based image analysis approach removes the time required for downloading, extracting and storing the images, is easily applicable to other regions, and reduces the amount of manual correction required,

https://doi.org/10.1017/jog.2023.18 Published online by Cambridge University Press

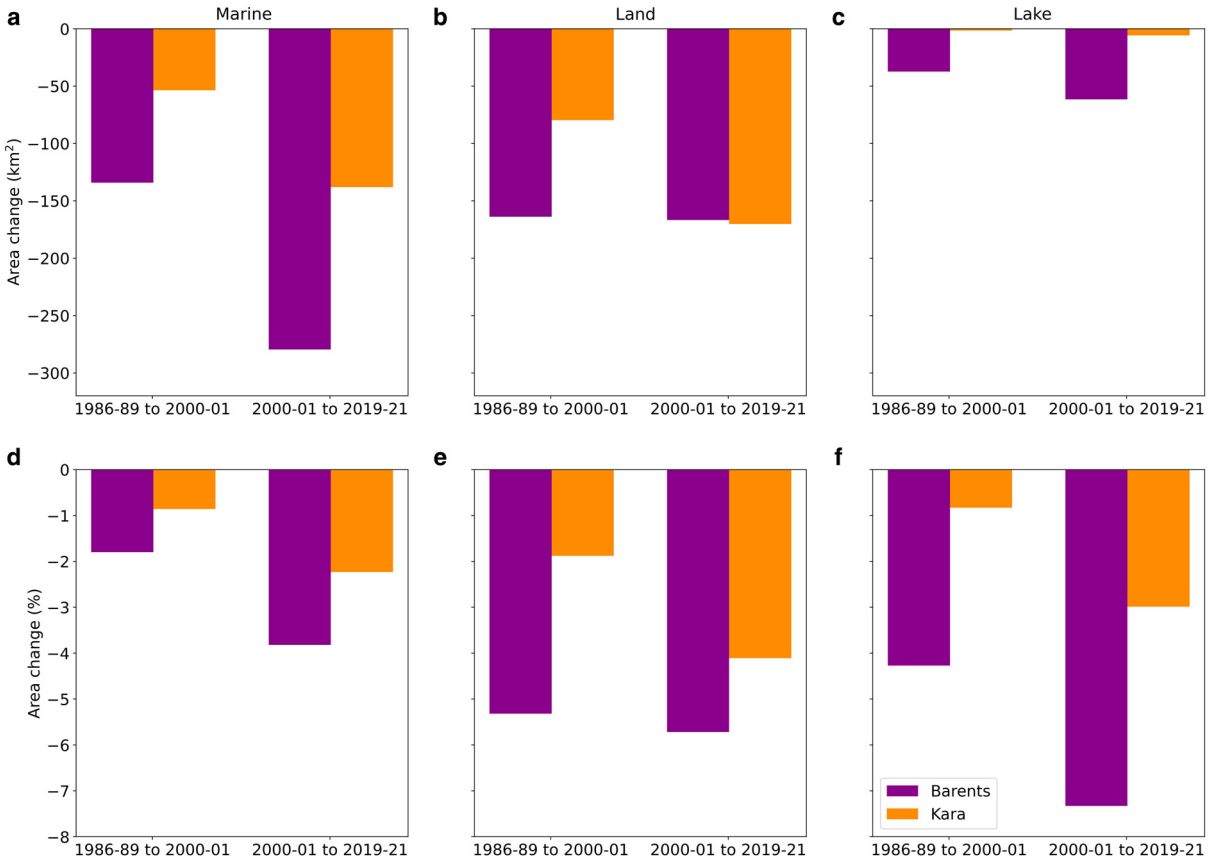

Figure 8. Area change of marine (a, d), land (b, e) and lake-terminating (c, f) glaciers on the Barents Sea vs Kara Sea, in km^2 (a–c) and per cent area (d–f).

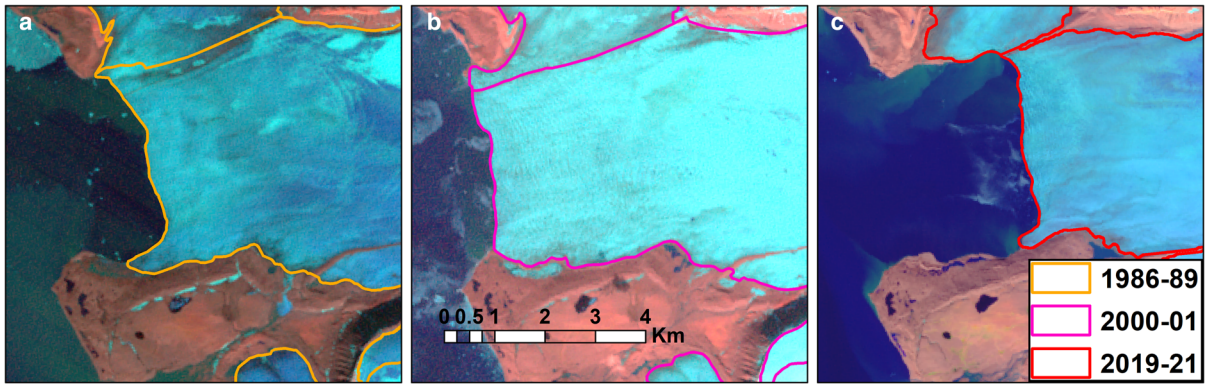

Figure 9. Time series of Landsat images showing Pavlov Glacier (RGI60-09.00070) in (a) 1986-07-26, (b) 2000-07-31 and (c) 2019-08-20, showing a clear advance associated with a surge between 1986 and 2000.

as compared to pixel-based methods. This method, however, may not be effective for mapping debris-covered glaciers, or areas covered by fresh snow or thin cloud cover. To address these issues, other approaches that have used object-based image analysis have included additional datasets such as DEMs and terrain slope or coherence derived from synthetic aperture radar images (Robson and others, 2015, 2016). Unfortunately, many of these products are not yet available in Google Earth Engine, though the possibility exists for users to upload and make use of these additional datasets in their workflows.

Conclusion

This study presents a new object-based image analysis methodology, implemented in Google Earth Engine, for rapid and accurate glacier mapping. The software framework designed in Google Earth Engine utilizes multi-temporal Landsat satellite imagery, and the outlines generated showed an accuracy of between 96 and 97% when compared to a manually corrected reference dataset. This demonstrates that our methodology is a powerful, robust tool for accurate and rapid mapping of glaciers changes on regional scale that reducing the time required of manual correction and can be applied to other glacierized regions. Utilizing this automated approach, we created outlines of glaciers on Novaya Zemlya for three different time periods: 1986–89, 2000–01 and 2019–21. This important dataset is essential for understanding the impact of climate change on glaciers, and could be used to estimate ice volume and mass change.

This method allowed for a comprehensive analysis of the changes that occurred in Novaya Zemlya glaciers between 1986–

https://doi.org/10.1017/jog.2023.18 Published online by Cambridge University Press

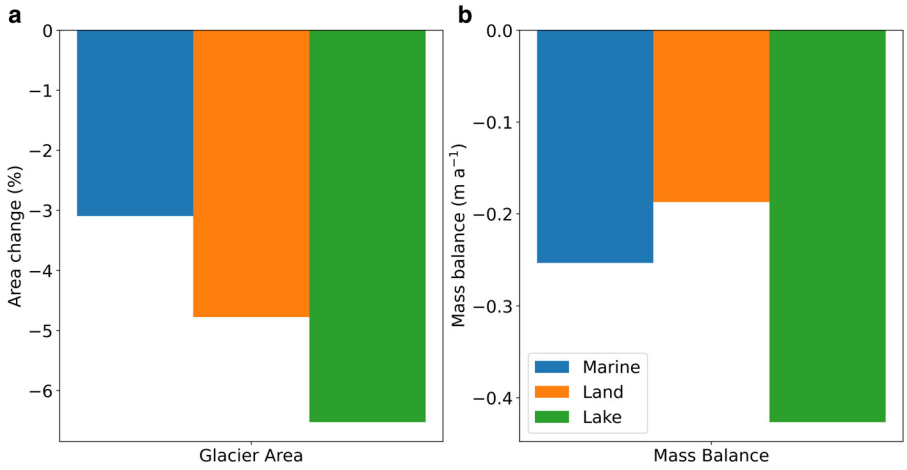

Figure 10. (a) Per cent area change (2000–01 to 2019–21) and (b) area-averaged mass change (2000–20) from Hugonnet and others (2021) for each glacier type.

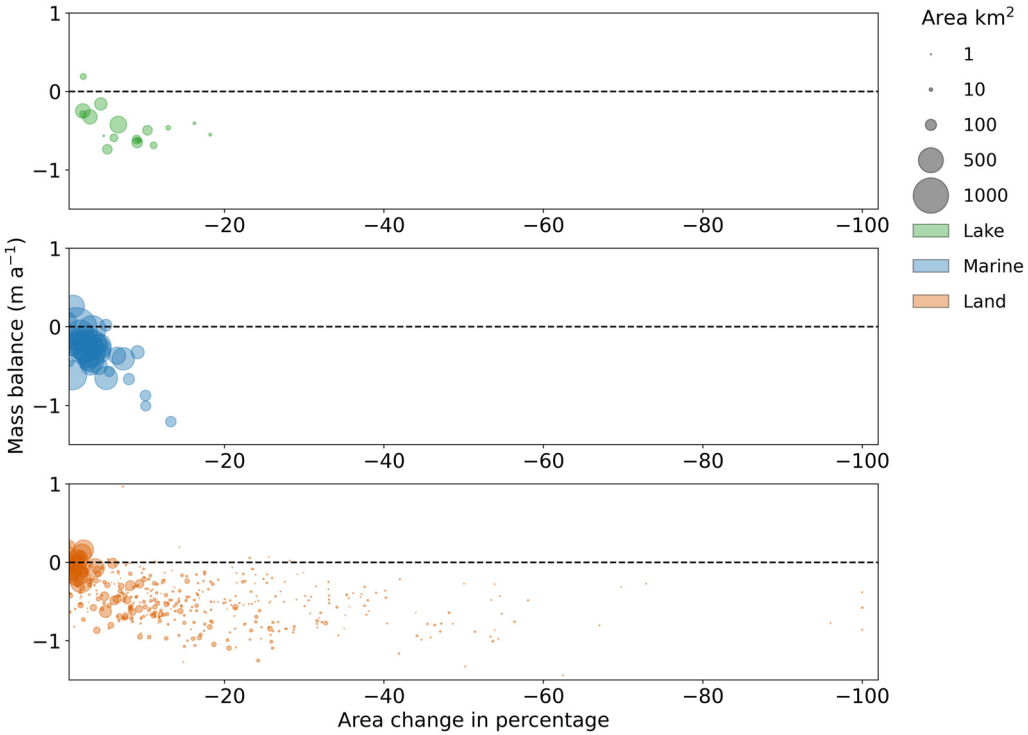

Figure 11. Area-averaged mass change (2000–20) from Hugonnet and others (2021) vs per cent area change (2000–01 to 2019–21) for each glacier.

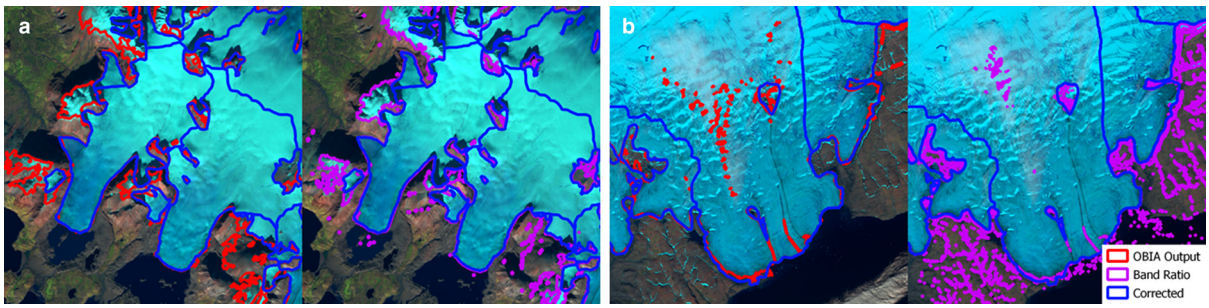

Figure 12. Comparison between object-based image analysis, band ratio and corrected outlines for two different sites in Novaya Zemlya.

89 and 2019–21. Over this time period, glaciers in Novaya Zemlya lost a total area of 1292 ± 419 km^2 (5.8%), with three glaciers disappearing entirely. The results clearly demonstrate that all glaciers in Novaya Zemlya are responding to the impacts of climatic warming in the Arctic. With the exception of four glaciers that surged between 1986–89 and 2000–01, all glaciers in the study area retreated between 1986–89 and 2019–21, and even those four glaciers have retreated since 2000–01.

https://doi.org/10.1017/jog.2023.18 Published online by Cambridge University Press

Our analysis indicates there are regional variations in how glaciers are responding to oceanic warming in this part of the Arctic, with more loss observed from glaciers that terminate on the Barents Sea side of Novaya Zemlya compared to those that terminate on the Kara Sea side. In comparison, results showed that land-terminating glaciers retreated less between 2000–01 and 2019–21 compared to 1986–89 and 2000–01, while the retreat rate of marine-terminating glaciers increased from 2000–01 to 2019–21, relative to 1986–89 to 2000–01. While marine-terminating glaciers, which cover the majority of Novaya Zemlya, lost more area than land- and lake-terminating glaciers, lake-terminating glaciers showed a larger percentage loss than the land- and marine-terminating glaciers.

Detailed regional studies of glacier behaviour across the Arctic are important for understanding the decadal responses and the likely trajectory of Arctic glaciers in a warming world. Given their potential contribution to global sea levels it is important to map and understand the scale of change accurately and to provide tools for rapid assessment at regional scales. Platforms such as Google Earth Engine, combined with the expansive Landsat archive and approaches such as object-based image analysis, help provide these tools.

Data. The manually corrected glacier outlines are available from the Global Land Ice Measurements from Space (GLIMS) database at http://www.glims.org/. An example Google Earth Engine script demonstrating the object-based image analysis process can be accessed at the following link: https://code.earthengine.google.com/?accept_repo=users/buner_shapfile/OBIA_Example_code.

Acknowledgements. This work was carried out as part of Asim Ali's PhD project, funded by an Ulster University Vice Chancellor's Research Studentship. Landsat images used in Google Earth Engine were provided by courtesy of the US Geological Survey. We thank James Lea, two anonymous reviewers and the editors for their constructive and insightful comments, which helped improve the quality of the manuscript.

Author contributions. AA developed the method, performed data analysis and interpretation, created figures and wrote the initial draft of the manuscript. PD, SC, DK and RM helped with conceptualization, methods, analysis and editing. RM also assisted with developing the method, creating figures and interpretation. RN helped with writing and editing the manuscript. All authors reviewed results and approved the final version of the manuscript.

References

Achanta R and Süsstrunk S (2017) Superpixels and polygons using simple non-iterative clustering. In *2017 IEEE Conference on Computer Vision and Pattern Recognition (CVPR)*, Honolulu, HI, pp. 4895–4904. doi:10.1109/CVPR.2017.520.

Albert TH (2002) Evaluation of remote sensing techniques for ice-area classification applied to the tropical Quelccaya Ice Cap, Peru. *Polar Geography* **26**(3), 210–226. doi:10.1080/789610193

Alifu H, Tateishi R and Johnson B (2015) A new band ratio technique for mapping debris-covered glaciers using Landsat imagery and a digital elevation model. *International Journal of Remote Sensing* **36**(8), 2063–2075. doi:10.1080/2150704X.2015.1034886

Amani M and 11 others (2020) Google Earth Engine cloud computing platform for remote sensing big data applications: a comprehensive review. *IEEE Journal of Selected Topics in Applied Earth Observations and Remote Sensing* **13**, 5326–5350. doi:10.1109/JSTARS.2020.3021052

AMAP (2017) *Snow, Water, Ice and Permafrost in the Arctic (SWIPA) 2017*. Arctic Monitoring and Assessment Programme (AMAP), Oslo, Norway.

Blaschke T (2010) Object based image analysis for remote sensing. *ISPRS Journal of Photogrammetry and Remote Sensing* **65**(1), 2–16. doi:10.1016/j.isprsjprs.2009.06.004

Bolch T, Menounos B and Wheate R (2010) Landsat-based inventory of glaciers in western Canada, 1985–2005. *Remote Sensing of Environment* **114**(1), 127–137. doi:10.1016/j.rse.2009.08.015

Burns P and Nolin A (2014) Using atmospherically-corrected Landsat imagery to measure glacier area change in the Cordillera Blanca, Peru from 1987 to 2010. *Remote Sensing of Environment* **140**, 165–178. doi:10.1016/j.rse.2013.08.026

Carr JR, Bell H, Killick R and Holt T (2017) Exceptional retreat of Novaya Zemlya's marine-terminating outlet glaciers between 2000 and 2013. *The Cryosphere* **11**(5), 2149–2174. doi:10.5194/tc-11-2149-2017

Carr JR, Stokes CR and Vieli A (2014) Recent retreat of major outlet glaciers on Novaya Zemlya, Russian Arctic, influenced by fjord geometry and sea-ice conditions. *Journal of Glaciology* **60**(219), 155–170. doi:10.3189/2014JoG13J122

Ciracì E, Velicogna I and Sutterley TC (2018) Mass balance of Novaya Zemlya archipelago, Russian High Arctic, using time-variable gravity from GRACE and altimetry data from ICESat and CryoSat-2. *Remote Sensing* **10**(11), 1817. doi:10.3390/rs10111817

Gorelick N and 5 others (2017) Google Earth Engine: planetary-scale geospatial analysis for everyone. *Remote Sensing of Environment* **202**, 18–27. doi:10.1016/j.rse.2017.06.031

Granshaw FD and Fountain AG (2006) Glacier change (1958–1998) in the North Cascades National Park Complex, Washington, USA. *Journal of Glaciology* **52**(177), 251–256. doi:10.3189/172756506781828782

Grant KL, Stokes CR and Evans IS (2009) Identification and characteristics of surge-type glaciers on Novaya Zemlya, Russian Arctic. *Journal of Glaciology* **55**(194), 960–972. doi:10.3189/002214309790794940

Hall DK, Riggs GA and Salomonson VV (1995) Development of methods for mapping global snow cover using moderate resolution imaging spectroradiometer data. *Remote Sensing of Environment* **54**(2), 127–140. doi:10.1016/0034-4257(95)00137-P

Hemati M, Hasanlou M, Mahdianpari M and Mohammadimanesh F (2021) A systematic review of Landsat data for change detection applications: 50 years of monitoring the earth. *Remote Sensing* **13**(15), 2869.

Hock R and 7 others (2019) GlacierMIP – a model intercomparison of global-scale glacier mass-balance models and projections. *Journal of Glaciology* **65**(251), 453–467. doi:10.1017/jog.2019.22

Hugonnet R and 10 others (2021) Accelerated global glacier mass loss in the early twenty-first century. *Nature* **592**(7856), 726–731. doi:10.1038/s41586-021-03436-z

IPCC (2021) *Climate Change 2021: The Physical Science Basis. Contribution of Working Group I to the Sixth Assessment Report of the Intergovernmental Panel on Climate Change*. Cambridge, UK, New York, USA: Cambridge University Press.

Isaksen K and 15 others (2022) Exceptional warming over the Barents area. *Scientific Reports* **12**(1), 9371. doi:10.1038/s41598-022-13568-5

Kääb AM and 11 others (2005) Remote sensing of glacier- and permafrost-related hazards in high mountains: an overview. *Natural Hazards and Earth System Sciences* **5**(4), 527–554. doi:10.5194/nhess-5-527-2005

Khan AA and 5 others (2020) Machine-learning algorithms for mapping debris-covered glaciers: the Hunza Basin case study. *IEEE Access* **8**, 12725–12734. doi:10.1109/ACCESS.2020.2965768

Kochtitzky W and Copland L (2022) Retreat of Northern Hemisphere marine-terminating glaciers, 2000–2020. *Geophysical Research Letters* **49**(3), e2021GL096501. doi:10.1029/2021GL096501.

Kohnemann SHE, Heinemann G, Bromwich DH and Gutjahr O (2017) Extreme warming in the Kara Sea and Barents Sea during the winter period 2000–16. *Journal of Climate* **30**(22), 8913–8927. doi:10.1175/JCLI-D-16-0693.1

Kulkarni AD and Lowe B (2016) Random forest algorithm for land cover classification. *International Journal on Recent and Innovation Trends in Computing and Communication* **4**(3), 58–63. doi:10.17762/ijritcc.v4i3.1834

Kulp SA and Strauss BH (2019) New elevation data triple estimates of global vulnerability to sea-level rise and coastal flooding. *Nature Communications* **10**(1), 4844. doi:10.1038/s41467-019-12808-z

Kumar M, Al-Quraishi AMF and Mondal I (2021b) Glacier changes monitoring in Bhutan High Himalaya using remote sensing technology. *Environmental Engineering Research* **26**(1), 190255. doi:10.4491/eer.2019.255

Kumar A, Yadav J and Mohan R (2021a) Spatio-temporal change and variability of Barents-Kara sea ice, in the Arctic: ocean and atmospheric implications. *The Science of the Total Environment* **753**, 142046.

Lea JM (2018) The Google Earth Engine digitisation tool (GEEDiT) and the margin change quantification tool (MaQiT) – simple tools for the rapid mapping and quantification of changing earth surface margins. *Earth Surface Dynamics* **6**(3), 551–561.

Liu X and 7 others (2018) High-resolution multi-temporal mapping of global urban land using Landsat images based on the Google Earth Engine

https://doi.org/10.1017/jog.2023.18 Published online by Cambridge University Press

platform. *Remote Sensing of Environment* **209**, 227–239. doi:10.1016/j.rse.2018.02.055

Ma L and 5 others (2019) Deep learning in remote sensing applications: a meta-analysis and review. *ISPRS Journal of Photogrammetry and Remote Sensing* **152**, 166–177. doi:10.1016/j.isprsjprs.2019.04.015

Mahdianpari M and 7 others (2020) Big data for a big country: the first generation of Canadian wetland inventory map at a spatial resolution of 10-m using Sentinel-1 and Sentinel-2 data on the Google Earth Engine cloud computing platform. *Canadian Journal of Remote Sensing* **46**(1), 15–33.

Masek JG and 6 others (2020) Landsat 9: empowering open science and applications through continuity. *Remote Sensing of Environment* **248**, 111968. doi:10.1016/j.rse.2020.111968

Melkonian AK, Willis MJ, Pritchard ME and Stewart AJ (2016) Recent changes in glacier velocities and thinning at Novaya Zemlya. *Remote Sensing of Environment* **174**, 244–257. doi:10.1016/j.rse.2015.11.001

Millan R, Mouginot J, Rabatel A and Morlighem M (2022) Ice velocity and thickness of the world's glaciers. *Nature Geoscience* **15**, 1–6. doi:10.1038/s41561-021-00885-z

Moon TA and 14 others (2019) The expanding footprint of rapid Arctic change. *Earth's Future* **7**(3), 212–218. doi:10.1029/2018EF001088

Nery T and 5 others (2016) Comparing supervised algorithms in land use and land cover classification of a Landsat time-series. In *2016 IEEE International Geoscience and Remote Sensing Symposium (IGARSS)*, Beijing, China, pp. 5165–5168. doi:10.1109/IGARSS.2016.7730346.

Nijhawan R, Garg P and Thakur P (2016) A comparison of classification techniques for glacier change detection using multispectral images. *Perspectives on Science* **8**, 377–380. doi:10.1016/j.pisc.2016.04.080

Nuth C (2013) Decadal changes from a multi-temporal glacier inventory of Svalbard. *The Cryosphere* **7**(5), 1603–1621. doi:10.5194/tc-7-1603-2013

Olofsson P, Foody GM, Stehman SV and Woodcock CE (2013) Making better use of accuracy data in land change studies: estimating accuracy and area and quantifying uncertainty using stratified estimation. *Remote Sensing of Environment* **129**, 122–131. doi:10.1016/j.rse.2012.10.031

Paul F and 24 others (2015) The glaciers climate change initiative: methods for creating glacier area, elevation change and velocity products. *Remote Sensing of Environment* **162**, 408–426. doi:10.1016/j.rse.2013.07.043

Paul F and 10 others (2017) Error sources and guidelines for quality assessment of glacier area, elevation change, and velocity products derived from satellite data in the Glaciers_CCI project. *Remote Sensing of Environment* **203**, 256–275. doi:10.1016/j.rse.2017.08.038

Paul F (2017) Glacier inventory. In Richardson D, Castree, N, Goodchild, MF, Kobayashi A, Liu W and Marston RA (eds), *International Encyclopedia of Geography*. John Wiley & Sons, Ltd., pp.1–12. doi:10.1002/9781118786352.wbieg0877.

Paul F, Kääb A and Haeberli W (2007) Recent glacier changes in the Alps observed by satellite: consequences for future monitoring strategies. *Global and Planetary Change* **56**(1), 111–122. doi:10.1016/j.gloplacha.2006.07.007

Paul F, Kääb A, Maisch M, Kellenberger T and Haeberli W (2002) The new remote-sensing-derived Swiss Glacier Inventory: I. methods. *Annals of Glaciology* **34**, 355–361. doi:10.3189/172756402781817941

Praticó S, Solano F, Di Fazio S and Modica G (2021) Machine learning classification of Mediterranean forest habitats in Google Earth Engine based on seasonal Sentinel-2 time-series and input image composition optimisation. *Remote Sensing* **13**(4), 586. doi:10.3390/rs13040586

Racoviteanu AE, Arnaud Y, Williams MW and Ordoñez J (2008) Decadal changes in glacier parameters in the Cordillera Blanca, Peru, derived from remote sensing. *Journal of Glaciology* **54**(186), 499–510. doi: 10.3189/002214308785836922

Racoviteanu AE, Paul F, Raup B, Khalsa SJS and Armstrong R (2009) Challenges and recommendations in mapping of glacier parameters from space: results of the 2008 Global Land Ice Measurements from Space (GLIMS) workshop, Boulder, Colorado, USA. *Annals of Glaciology* **50**(53), 53–69. doi:10.3189/172756410790595804

Rantanen M and 7 others (2022) The Arctic has warmed nearly four times faster than the globe since 1979. *Communications Earth & Environment* **3**(1), 1–10. doi:10.1038/s43247-022-00498-3

Rastner P, Bolch T, Notarnicola C and Paul F (2013) A comparison of pixel-and object-based glacier classification with optical satellite images. *IEEE Journal of Selected Topics in Applied Earth Observations and Remote Sensing* **7**(3), 853–862.

Rastner P, Strozzi T and Paul F (2017) Fusion of multi-source satellite data and DEMs to create a new glacier inventory for Novaya Zemlya. *Remote Sensing* **9**(11), 1122. doi:10.3390/rs9111122

Raup BH and 5 others (2007) The GLIMS geospatial glacier database: a new tool for studying glacier change. *Global Planetary Change* **56**(1–2), 101–110. doi:10.1016/j.gloplacha.2006.07.018

Ren X and Malik J (2003) Learning a classification model for segmentation. In *Proceedings Ninth IEEE International Conference on Computer Vision*. Vol. 1, Nice, France, pp. 10–17. doi:10.1109/ICCV.2003.1238308.

RGI Consortium (2017) Randolph Glacier Inventory 6.0. doi: 10.7265/N5-RGI-60.

Robson BA and 5 others (2015) Automated classification of debris-covered glaciers combining optical, SAR and topographic data in an object-based environment. *Remote Sensing of Environment* **170**, 372–387. doi:10.1016/j.rse.2015.10.001

Robson BA, Hölbling D, Nuth C, Strozzi T and Dahl SO (2016) Decadal scale changes in glacier area in the Hohe Tauern National Park (Austria) determined by object-based image analysis. *Remote Sensing* **8**(1), 67. doi:10.3390/rs8010067

Schädel C and 14 others (2018) Divergent patterns of experimental and model-derived permafrost ecosystem carbon dynamics in response to Arctic warming. *Environmental Research Letters* **13**(10), 105002. doi:10.1088/1748-9326/aae0ff

Shafizadeh-Moghadam H, Khazaei M, Alavipanah SK and Weng Q (2021) Google Earth Engine for large-scale land use and land cover mapping: an object-based classification approach using spectral, textural and topographical factors. *GIScience & Remote Sensing* **58**(6), 914–928. doi:10.1080/15481603.2021.1947623

Sharp M and 12 others (2014) Remote sensing of recent glacier changes in the Canadian Arctic. In Kargel JS, Leonard GJ, Bishop MP, Kääb A and Raup BH (eds.), *Global Land Ice Measurements from Space*. PUBLOCBerlin, Heidelberg: Springer Berlin Heidelberg, pp. 205–228. doi:10.1007/978-3-540-79818-7_9.

Tassi A and Vizzari M (2020) Object-oriented LULC classification in Google Earth Engine combining SNIC, GLCM, and machine learning algorithms. *Remote Sensing* **12**(22), 3776. doi:10.3390/rs12223776

Winsvold SH, Andreassen LM and Kienholz C (2014) Glacier area and length changes in Norway from repeat inventories. *The Cryosphere* **8**(5), 1885–1903. doi:10.5194/tc-8-1885-2014

Wulder MA and 26 others (2022) Fifty years of Landsat science and impacts. *Remote Sensing of Environment* **280**, 113195. doi:10.1016/j.rse.2022.113195

Xue X and 7 others (2018) Delineating urban boundaries using Landsat 8 multispectral data and VIIRS nighttime light data. *Remote Sensing* **10**(5), 799. doi:10.3390/rs10050799

Yamagami Y, Watanabe M, Mori M and Ono J (2022) Barents–Kara sea-ice decline attributed to surface warming in the Gulf Stream. *Nature Communications* **13**(1), 1–10.

You Q and 15 others (2021) Warming amplification over the Arctic Pole and Third Pole: trends, mechanisms and consequences. *Earth-Science Reviews* **217**, 103625. doi:10.1016/j.earscirev.2021.103625

Zemp M and 14 others (2019) Global glacier mass changes and their contributions to sea-level rise from 1961 to 2016. *Nature* **568**(7752), 382–386. doi:10.1038/s41586-019-1071-0

Zhang X and 6 others (2020) Development of a global 30 m impervious surface map using multisource and multitemporal remote sensing datasets with the Google Earth Engine platform. *Earth System Science Data* **12**(3), 1625–1648.

https://doi.org/10.1017/jog.2023.18 Published online by Cambridge University Press